

Interfacial Energy Transfer during Gamma Radiolysis of Water on the Surface of ZrO₂ and Some Other Oxides

N. G. Petrik,^{†,‡,*} A. B. Alexandrov,^{†,‡,§} and A. I. Vall^{||}

W. R. Wiley Environmental Molecular Sciences Laboratory, Pacific Northwest National Laboratory, P.O. Box 999, Richland, Washington 99352; All-Russian Project and Research Institute of Complex Power Technology, 55 Dibunovskaja St., St.Petersburg 197228, Russia; and Institute of Technology, 26 Moscovsky Av., St.Petersburg 198013, Russia

Received: December 7, 2000; In Final Form: April 9, 2001

The effect of an oxide interface on ⁶⁰Co gamma radiolysis of water molecules was studied. On the basis of the molecular hydrogen yield when compared with the radiolysis of the control ampules without oxides, all the tested materials can be generally classified into three groups: I. Oxides that lower the H₂ yield (MnO₂, Co₃O₄, CuO, and Fe₂O₃); II. Oxides with H₂ yields that are close to G values obtained in control experiments (MgO, CaO, SrO, BaO, ZnO, CdO, Cu₂O, NiO, Cr₂O₃, Al₂O₃, CeO₂, SiO₂, TiO₂, Nb₂O₅ and WO₃); and III. Oxides that can increase the H₂ yield as compared with the radiolysis of water without oxides (Ga₂O₃, Y₂O₃, La₂O₃, Nd₂O₃, Sm₂O₃, Eu₂O₃, Gd₂O₃, Yb₂O₃, Er₂O₃, HfO₂, and ZrO₂). For the third group, the H₂ yield can be much greater than for the homogeneous process due to effective energy transfer at the oxide/water interface. There are several parameters, such as the oxide band-gap, water adsorption form, and energy migration distance that can collectively contribute to “enhanced” radiolysis yields at interfaces. We present data of “effective” H₂ yield vs band-gap (*E_g*) energy that show a resonant maximum at *E_g* = 5 eV. This maximum corresponds to the energy of H–OH bond in the water molecule (5.1 eV). By varying the ZrO₂ specific area within a 0.02–12 m² g⁻¹ range, we also demonstrated that the H₂ yield per unit area of the crystal surface is constant. Doping the ZrO₂ bulk with Nb⁵⁺ and Li⁺ ions has a remarkable effect on the H₂ yield from the surface. We estimated the energy migration distance to be ~5 nm. Thermally stimulated luminescence was used to probe the nature of the migrating electronic excitations in ZrO₂. Finally, we propose a mechanism for the adsorbed water radiolysis based on the migration of excitons to the surface and their resonant coupling with the H₂O/oxide adsorption complex.

1. Introduction

Irradiation of heterogeneous systems often leads to an effective redistribution of absorbed radiation energy between contacting phases. This very important and interesting feature has received relatively little attention.^{1–10} The energy of ionizing radiation absorbed in one phase can be delivered to the interface and can induce physical and chemical processes in the other phase. The energetic efficiency of the adsorbed molecule radiolysis (i.e., radiation-chemical yield) should be attributed to the energy absorbed by the molecules both directly and indirectly (i.e., delivered from the adsorbent). Energy redistribution in heterogeneous systems, which is very important for radiation catalysis, also is significant in material surface sciences since it allows control of radiation-induced corrosion in many metal, glass, ceramic, and semiconductor materials.

In general, radiation energy redistribution in heterogeneous systems consists of two stages: (1) energy migration from the bulk to interface and (2) energy transfer through the interface

from one phase to another phase. Usually, a primary absorption event involving a highly energetic particle or quantum (e.g., α , β , γ) energy absorption and a final radiation-induced chemical reaction event are separated in space and time. The energy migration between these points in condensed phases is conducted mostly by the highly energetic secondary electrons (~10² to 10⁵ eV); intermediate energy, nonthermal, or “hot” carriers (~0.1 to 100 eV); and thermalized particles or excitations (<0.1 eV).

For heterogeneous systems, the imbalance between secondary electron fluxes in both directions through the interface for systems with different density and atomic composition can lead to a higher dose rate for the adsorbed molecules in comparison to irradiation of the homogeneous molecular systems. Intermediate energy electrons (10 to 100 eV) have very short inelastic mean free path (0.3 to 2 nm),¹¹ and they can contribute to surface reactions from just a few subsurface atomic layers. “Hot” carriers can migrate further; for example, a “hot” hole in oxides can diffuse to the surface from 50 to 250 nm.¹² The lifetime of thermalized electronic excitations in perfect, defect-free crystals can be long enough to provide much longer distances of migration—up to hundreds of micrometers.^{3,5,13,14}

For oxides, an interfacial energy transfer was observed for radiolysis of N₂O adsorbed on ZrO₂ and SiO₂,⁸ Al₂O₃, and MgO;^{15–18} H₂O adsorbed on ZrO₂, Er₂O₃, and La₂O₃;¹⁹ methanol adsorbed on ZrO₂, CaO, Al₂O₃, MgO, and SiO₂;⁹ NO₃⁻

* To whom correspondence should be addressed. E-mail: Nikolai.Petrik@pnl.gov. Fax: (509)376-6066.

[†] W. R. Wiley Environmental Molecular Sciences Laboratory, Pacific Northwest National Laboratory.

[‡] All-Russian Project and Research Institute of Complex Power Technology.

[§] Current address: School of Chemistry and Biochemistry, Georgia Institute of Technology, Atlanta, GA 30332-0400.

^{||} Institute of Technology.

and azoethane adsorbed on MgO.^{6,10} The mechanism for energy transfer is not well understood. Three major models typically are discussed: hole-electron (or electron-hole) recombination on the adsorbed molecule, dissociative electron attachment, and resonance exciton coupling.

There is a large amount of literature concerning photocatalytic splitting of water on TiO₂ and other oxide surfaces (see for example^{20–25}). The formation of H₂ and O₂ results from electron-hole pair creation, separation, and reaction of the separated charge carriers with water on the oxide surface loaded with special catalysts (e.g., Pt, RuO₂, etc.). Bare (not loaded) TiO₂ is not active in water photocatalytic splitting.^{20–23} Sayama et al.^{22,23} showed that 4.88 eV (254 nm) UV light does not dissociate water in suspension with TiO₂ and Ta₂O₅. Rather, it creates electron-hole pairs in these oxides, having band gaps of 3 and 4 eV, respectively. The same UV light decomposes water to H₂ and O₂ on the surface of ZrO₂. However, the efficiency of electron-hole pair production is low in this oxide with a 5 eV band gap. Hence, an electron-hole separation is not the only mechanism for water photocatalytic splitting on oxide surfaces.

A goal of the study described in this paper was to investigate the main factors that affect energy transfer in the oxide/water system under gamma irradiation. We report on radiolysis of H₂O molecules adsorbed on ZrO₂ and some other oxide powders as a function of the oxide (band gap, crystal size, dopant type, and concentration) and adsorbate (surface concentration, adsorption form) parameters. We suggest that an exciton mechanism drives energy transfer from ZrO₂ to the water adsorption complex. We had reported some of our preliminary data elsewhere.^{4,26}

In section II, we describe the general experimental approach, and in section III, we present survey results on the gamma radiolysis of water adsorbed on the surface of MgO, CaO, SrO, BaO, ZnO, CdO, CuO, Cu₂O, Al₂O₃, Ga₂O₃, Y₂O₃, La₂O₃, Nd₂O₃, Sm₂O₃, Eu₂O₃, Gd₂O₃, Yb₂O₃, Er₂O₃, CeO₂, SiO₂, TiO₂, ZrO₂, HfO₂, Nb₂O₅, Cr₂O₃, WO₃, MnO₂, NiO, Co₃O₄, and Fe₂O₃ microcrystalline samples. Results on more detailed studies of water radiolysis over the pure ZrO₂ and ZrO₂ doped with Nb⁵⁺ or Li⁺ are presented in section III. Finally, in section IV, we present a summary of the possible mechanisms and discuss several of the overall parameters that should be considered when addressing radiolysis of water on oxide surfaces. The relevance to radiolysis of heterogeneous systems is also addressed.

2. Experimental Section

The following powdered, ultrapure grade crystal oxides were tested in our study: MgO, CaO, SrO, BaO, ZnO, CdO, CuO, Cu₂O, Al₂O₃, Ga₂O₃, Y₂O₃, La₂O₃, Nd₂O₃, Sm₂O₃, Eu₂O₃, Gd₂O₃, Yb₂O₃, Er₂O₃, CeO₂, SiO₂, TiO₂, ZrO₂, HfO₂, Nb₂O₅, Cr₂O₃, WO₃, MnO₂, NiO, Co₃O₄, and Fe₂O₃. For TiO₂, ZrO₂, MgO, Cr₂O₃, CuO, and SiO₂, we used several different stocks of a given oxide with different characteristics (purity, grain size, specific area, etc.). The total concentration of impurities was less than 0.01 mol % for most of the oxides (<0.001% for ZrO₂). X-ray photoelectron spectroscopy and Auger electron spectroscopy were used to characterize the oxide surfaces. Usually, small amounts of carbon-containing organic contaminants were detected on the oxide surface.

X-ray diffraction analysis of ZrO₂ showed a monoclinic crystal structure, which is the basic structure for zirconia at room temperature. To dope the ZrO₂ with Li⁺ and Nb⁵⁺, we used water solutions of LiNO₃ and Nb(NO₃)₃. A given amount of the dopant solution was distributed uniformly on the powder

surface, and the sample then was dried and subjected to long-term diffusion annealing for 10 h at 1300 K in air. The reference sample was treated with the same procedure, but no metals were present in the water solution. ZrO₂ and TiO₂ were studied as powdered crystal materials and as 0.05 to 5 mm microcrystals. The crystals were synthesized at the A. Ioffe Institute of Physics and Technics (St. Petersburg, Russia) using a noncrucible induction melting method. SiO₂ was studied in three different forms: silica gel “KSK” (~300 m²/g), ultrahigh purity amorphous SiO₂, and crystal (α -quartz) SiO₂ with grain sizes ranging from 0.05 to 10 mm. The ultrahigh pure SiO₂ samples were synthesized at the Institute of Quartz Glass, St. Petersburg, Russia. The specific area of the oxides was determined utilizing the standard Brunauer-Emmett-Teller (BET) method, which involves low-temperature (77 K) adsorption of N₂, Ar, or Xe.²⁷ The oxides were thermal treated up to 773 K in helium gas prior to surface measurement.

Typically, we placed a portion of oxide sample into a Pyrex glass ampule and heated it to 773 K under 10⁻² Pa vacuum for 10 to 20 min. Some of the MeO-type oxides (e.g., MgO, CaO, CdO, etc.) developed hydroxide inclusions after contact with the atmosphere. We then subjected the samples to a 1000 to 1300 K thermal treatment for several hours prior the water dosage. The oxide surface area was measured after the high-temperature treatment. The water dosage system allowed us to introduce a constant volume (1.0 cm³) of H₂O vapor from the “premixing” reservoir into the ampule. Degassed, double-distilled water was used to create a wide range of the vapor pressures in the vacuumized “premixing” reservoir. The water vapor was dosed into the ampule containing the oxide sample. The oxide samples were kept in contact with the water vapor for 1 day to ensure an equilibrium adsorption. The temperature conditions ranged from liquid nitrogen to ambient laboratory temperatures. The ampule with dosed water and oxide was sealed, cooled, irradiated, and analyzed for molecular hydrogen. A “reference” ampule contained a dose of water without an oxide. The temperature-programmed desorption (TPD) of water experiments were conducted at a linear heating rate of 1 K/s from 80 to 770 K. We monitored the pressure over the oxide sample under a constant pumping. The samples were treated thermally prior to the water adsorption step. Our control experiments did not show any gases desorbing from the “dry” surface. The absolute amount of adsorbed water was measured by the Penfield method,²⁸ which is based on the thermal desorption of water from the surface at 770 K, water condensation in a fine glass capillary, and differential weight measurements.

The samples were irradiated with 1.25-MeV gamma quanta in the ⁶⁰Co irradiation facility at the Institute of Technology, in St. Petersburg, Russia. The temperature during irradiation was 315 ± 5 K, and the absorbed dose rate was 1.8 ± 0.15 Gy/s, as determined by Fricke dosimetry.²⁹ The absorbed dose ranged from 0.1 to 1.5 MGy (MJ/kg).

Molecular hydrogen was analyzed using gas chromatography and a thermocatalytic detector. The determination threshold was better than 1 nmol/probe.

Thermoluminescence (TL) of the irradiated samples was measured at the TSL-K facility designed at the Physics Institute of the Latvian Academy of Science. Crystals were heated using a tantalum resistive heater at a 1 K/s linear temperature ramping rate in the region of 300 to 770 K. The temperature uncertainty was ±20 K for the largest crystals (2 to 3 mm). Emission was detected in the 400 to 620 nm region by an FEU-71 photomultiplier tube equipped with an Sb-Cs photocathode.

3. Results

A. Effect of the Oxide Interface on the Radiolytical Decomposition of Adsorbed Water. The effect of the oxide interface on the radiolytical decomposition of adsorbed water was determined by comparing of the H_2 yields from the adsorbed water and from the homogeneous water vapor. Two variations of water dosage were used for most of the oxides studied:

1. Equal amounts of water were dosed into the ampules with various oxides (0.02 to 0.5 mmol/gram of oxide for different experimental series).

2. Different amounts of water were dosed into the ampules to provide a surface coverage close to one monolayer ($(0.6 \text{ to } 1.0) \times 10^{19}$ molecules/ m^2). The oxide surface area varied from 0.5 to 290 m^2/g .

To compare data obtained for homogeneous and heterogeneous water, the hydrogen yields were calculated on an electron fraction basis relative to the fraction of gamma-ray energy directly absorbed by the H_2O molecules.^{29,30} If the numbers exceeded the "homogeneous" $G(H_2)$ values, an energy transfer from the substrate would be expected. $G(H_2)$ is an "observed" radiation-chemical yield of hydrogen, experimentally measured after the irradiation. $G(H_2)$ is not a constant and relates to the primary and secondary processes producing and decomposing the hydrogen molecules.^{30,31} $G(H_2)$ is very dependent on the various experimental conditions. For pure water we can assume $G(H_2) < G_{H_2} + 0.5(G_H + G_{e^-})$ where G_{H_2} , G_H , and G_{e^-} are the "primary" radiation-chemical yields of H_2 , H and e^- respectively.^{30,31} Therefore, for the γ -irradiation we can estimate $G(H_2) < 4 (100 \text{ eV})^{-1}$ for the vapor water and $G(H_2) < 2.2 (100 \text{ eV})^{-1}$ for the liquid water according to the data from Ref 31,32. For a very pure reservoir with water vapor, $G(H_2)$ can be as low as $0.007 (100 \text{ eV})^{-1}$.³³ Depending on the referencing oxide sample, a control ampule contained 1 to 60 μmol water as a vapor or liquid/vapor mixture. After irradiation with doses ranging from 0.1 to 1.5 MGy, we obtained $G(H_2)$ control values that ranged from 0.1 to 3 $(100 \text{ eV})^{-1}$, depending on the water amount, dose, ampule condition, and other experimental parameters.

Ampules that contained oxides showed various H_2 yields, and according to the radiation-chemical yields, the oxides can be generally classified into three groups:

1. Oxides that lower the H_2 yield (shown in parentheses as molecules/100 eV) as compared with the radiolysis of the control ampules that did not contain oxides. This group includes MnO_2 (0.002 to 0.04), Co_3O_4 (0.001 to 0.06), CuO (0.001 to 0.08), and Fe_2O_3 (0.09).

2. Oxides with H_2 yields that are close to G values obtained in our control experiments. This group includes MgO (1.3 to 1.9), CaO (0.2 to 1.4), SrO (0.4 to 2.4), BaO (0.3 to 3.3), ZnO (0.1 to 1.8), CdO (0.2 to 3.0), Cu_2O (0.2 to 3.0), NiO (0.3 to 0.4), Cr_2O_3 (0.1 to 2.0), Al_2O_3 (0.2), CeO_2 (2.6), SiO_2 (1.0 to 3.0), TiO_2 (0.3 to 0.5), V_2O_5 (0.2 to 1.0), Nb_2O_5 (0.2 to 0.4) and WO_3 (0.4).

3. Oxides that can increase the H_2 yield as compared with the radiolysis of water without oxides. This group includes Ga_2O_3 (30), Y_2O_3 (4 to 20), La_2O_3 (10), Nd_2O_3 (3.0 to 5.5), Sm_2O_3 (3 to 15), Eu_2O_3 (6 to 40), Gd_2O_3 (4 to 6), Yb_2O_3 (6 to 10), Er_2O_3 (10 to 140), HfO_2 (10), and ZrO_2 (10 to 80). These numbers do not reflect a real energetic efficiency of the radiolysis and should be attributed to the effective energy transfer at the oxide/water interface.

Figure 1 shows the amount of hydrogen produced vs the absorbed gamma dose for 20 μmol of water in the vapor phase and for the same amount of water adsorbed on the ZrO_2 surface

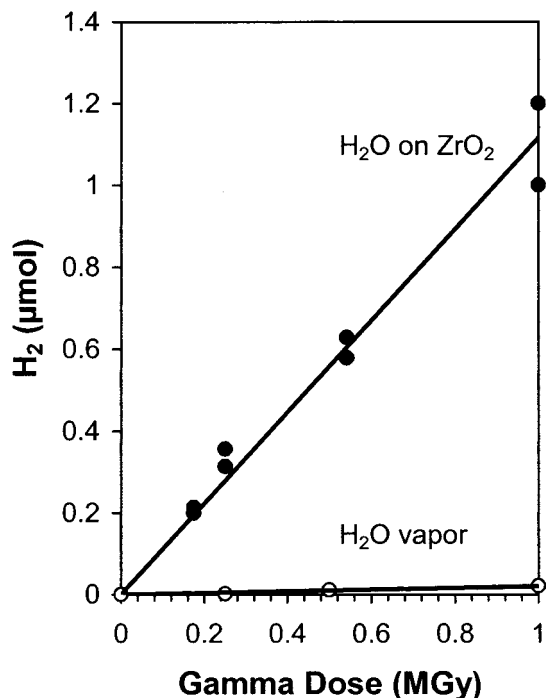


Figure 1. Amount of the produced hydrogen vs absorbed gamma dose for radiolysis of 20 μmol of water in vapor phase and 20 μmol of water adsorbed on the ZrO_2 surface with coverage of ~ 10 molecule/ nm^2 .

at coverage of 10 molecule/ nm^2 . The H_2 dose dependence is linear. The H_2 production from the adsorbed water is about 2 orders of magnitude higher than from the water vapor.

Typically, the hydrogen yield shows quite a broad distribution for various experimental conditions: the oxide stock, the sample pretreatment, the water coverage, and the dosage procedure, the absorbed gamma-dose, etc. For that reason, we did not average the presented above data taken under different conditions. The effect of some of these parameters on the heterogeneous radiolysis of water was studied predominately for ZrO_2 as it is one of the most effective promoters of H_2 production.

B. Effect of the Water Adsorption Form on the H_2 Yield.

Adsorption can remarkably change the electronic structure and the bond energy of the water molecule and even can dissociate it.³⁴ Thus, different forms of water adsorption may have different dissociation thresholds. Figures 2 and 3 show H_2 yields from the ZrO_2 surfaces (12 m^2/g) that were exposed to water vapor at 77 K and heated to a given temperature for 10 min. Such treatment leads to a selective desorption of different water adsorption forms. Our choice of the duration of thermal treatment was based on data presented in the Figure 2c. After this procedure, the ampule with the sample was sealed, brought to the room temperature, and irradiated at 315 K.

Figure 3b shows the TPD of water multilayers from a ZrO_2 powder surface. A sharp peak from physisorbed water (200 to 250 K) and two broad peaks from chemisorbed water at ~ 400 K and 550 to 600 K are observed. Other oxides exhibit different temperatures for the TPD peaks for chemisorbed water and different ratios between different states of water. For Me_2O_3 - MeO_3 oxides, the maximal total surface coverage with the chemisorbed water was 8 to 10 molecules/ nm^2 , which is close to one monolayer. For ZrO_2 , after extended exposure to saturated water vapor at 300 K, vacuum pumping, and desorption of physisorbed water, the total amount of chemisorbed water was 8 ± 1.5 molecules/ nm^2 . Of this total, ~ 4 molecules/ nm^2 desorbs in the 300 to 473 K region, and the remaining ~ 4 molecules/ nm^2 desorbs in the 473–773 K region (as measured by the

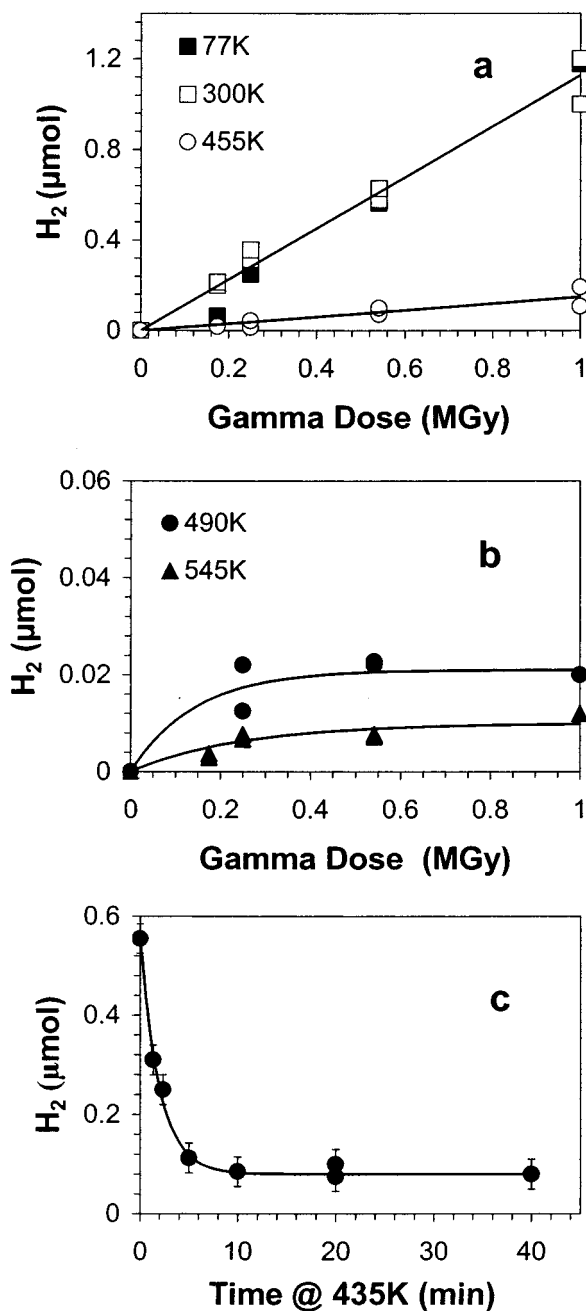


Figure 2. Hydrogen production vs absorbed gamma dose (a, b) for radiolysis of H_2O molecules dosed on the ZrO_2 surface at 77 K and selectively desorbed at different temperatures in a vacuum (labels). The irradiation temperature is 315 K. (c): H_2 production vs time of the isothermal pretreatment. H_2O was dosed on the ZrO_2 surface and then desorbed at 435 K for different time. $D_\gamma = 0.5$ MGy.

Penfield method²⁸). In addition to the chemisorbed water, one monolayer (~ 10 molecules/ nm^2) of the physisorbed water covers the surface after the dosing at 77 K, sealing the ampule, and bringing it to the irradiation temperature (see filled squares in Figure 2a). This result agrees with the published adsorption isotherm for H_2O on ZrO_2 .^{27,35,36}

A dramatic decrease of the hydrogen yield occurs after the heat treatment at 455 K (Figure 3a). Hence, a dominant part of the hydrogen relates to the first form of the chemisorbed water (TPD maximum at ~ 400 K). The hydrogen yield corresponding to this state of water (see Figure 3A) is as high as 75 ± 10 (100 eV)⁻¹. Hydrogen yield for the high-temperature form is 1 to 2 (100 eV)⁻¹. The energy transfer to the physisorbed H_2O

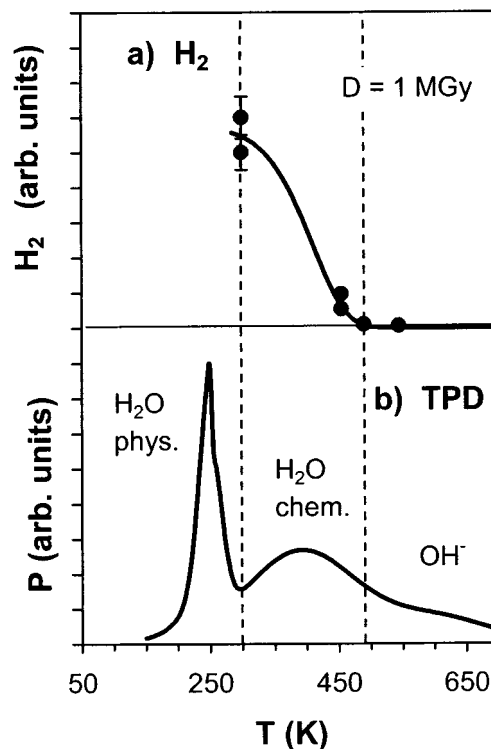


Figure 3. (a) Hydrogen production vs temperature of isothermal pretreatment for radiolysis of H_2O molecules dosed on the ZrO_2 surface. $D_\gamma = 1.0$ MGy. The data are taken from Figure 2. (b) TPD of water from ZrO_2 surface during thermal pretreatment.

molecules does not seem to be effective (compare filled and empty squares in Figure 2a).

A similar interpretation can be given to data on water dosing on the ZrO_2 surface that has been de-hydrated at 773 K. Small amounts of the dosed water (~ 0.1 ML), adsorbed most likely in the high-temperature state, produce very little hydrogen under subsequent irradiation (< 0.2 nmol of H_2 from $1.1 \mu\text{mol}$ of H_2O at 0.75 MGy). At higher surface coverage (~ 0.5 ML), this state saturates, and the low-temperature chemisorption state populates, which leads to a remarkable increase of the hydrogen yield (540 nmol of H_2 from $5.5 \mu\text{mol}$ of H_2O at the same dose).

Thus, the efficiency of the energy transfer to the adsorbed water molecules is extremely sensitive to the H_2O molecule adsorption form.

C. Effect of the ZrO_2 Dispersion on the H_2 Yield. The distance of energy migration to the surface is limited and can be evaluated by changing the sample dispersion.^{3,8,14} For an interfacial process driven by migration of electronic excitations from the bulk to the surface, the yield will be maximal when all the excitations, which are created in the bulk, are able to reach the surface during their lifetime. This happens when an average displacement of the migrating excitation is equal to or higher than a nominal crystal size.

ZrO_2 crystals (see the Experimental Section) were crushed and separated using a number of sieves in the range from 0.05 to 5 mm. Finally, the samples were stabilized by annealing in air at 1300 K for 10 h. Specific area was measured for each sample. One monolayer of water was dosed onto each sample, and they were irradiated with the same gamma dose.

Figure 4 illustrates the dependence of H_2 yields on the ZrO_2 specific area. Hydrogen yield increases in direct proportion to the specific area for all the crystal sizes (a dashed line is a linear approximation). There is a slight tendency to saturation at the highest level of dispersion. Thus, the lowest nominal crystal

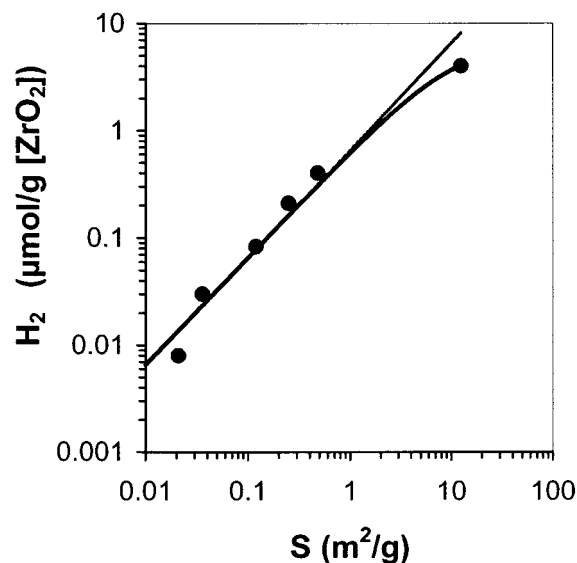


Figure 4. H₂ production per gram of ZrO₂ vs oxide specific area. H₂O coverage is 1 ± 0.2 ML. $D_\gamma = 0.25$ MGy.

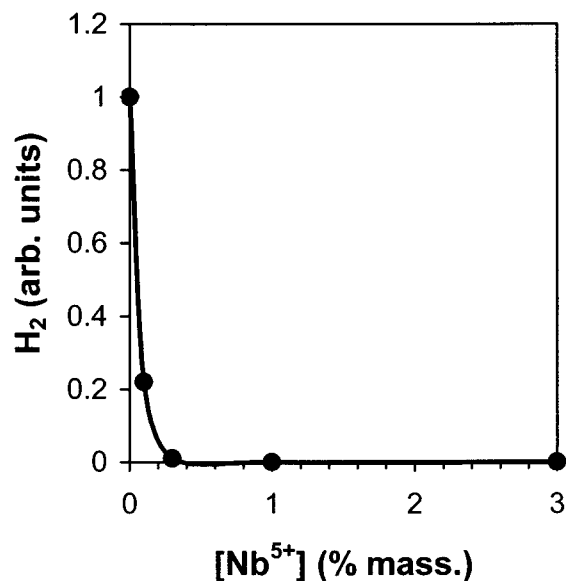


Figure 5. H₂ production per gram of ZrO₂ vs concentration of Nb⁵⁺ in ZrO₂. $D_\gamma = 0.5$ MGy. H₂O coverage is 1 ± 0.2 ML.

size for the sample with $S = 12 \text{ m}^2 \text{ g}^{-1}$ is much greater than the energy migration distance.

D. Effect of the ZrO₂ Doping on the H₂ Yield. A “bulk-surface” energy exchange also could be affected by doping the oxide crystal lattice. Doping can create additional traps for migrating electronic excitations, thus decreasing their lifetime and, therefore, their diffusion path and displacement. Doping with different cations also can effect the equilibrium concentration of structure defects (e.g., oxygen vacancies) and charge carriers (electrons, holes).³⁷

For an easy substitution of Zr⁴⁺ cation in the lattice site, the Nb⁵⁺ ion was chosen as a dopant because of its neighboring position in the Periodic Table and its similar electronic structure. Figure 5 shows the effect of doping ZrO₂ with Nb⁵⁺ ions on the H₂ yield. Quite small concentrations ($\sim 0.1\%$ mass.) of the dopant cations in the bulk of ZrO₂ significantly suppress radiolysis of water adsorbed on the surface. On the other hand, doping ZrO₂ with 0.1% mass of single-charged cations Li⁺ or Rb⁺ promotes the H₂ production by a factor of 2. The effect of doping is consistent with low energy electronic excitations

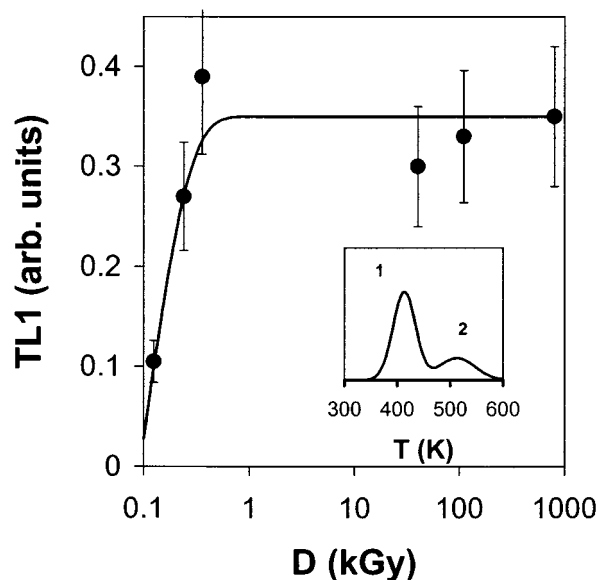


Figure 6. TL yield for peak (1) (see inset) vs absorbed gamma-dose for 0.25–0.5 mm ZrO₂ microcrystals. Inset: thermoemission curve for gamma irradiated ZrO₂ microcrystals. Peaks 1 and 2 are labeled. $D_\gamma = 0.24$ kGy.

involved in water dissociation, because all alternative mechanisms, based on the secondary electron emission, would not be so sensitive to such relatively low concentrations of the dopant.

Therefore, defects in the oxide crystal lattice and their structure are other factors that control radiolysis of water adsorbed on the surface of ZrO₂.

E. Effect of the Oxide Dispersion and Doping on the Stored Energy accumulation. Thermoluminescence of Irradiated ZrO₂ Microcrystals. In general, radiation energy absorbed by solids eventually dissipates into three main channels: thermal, defects, and luminescence. Energy expended on defect creation typically is considered to be stored. For disperse systems, an additional channel—surface reaction—is important. Experiments with heterogeneous systems often show a competition between surface reactions and other channels of energy dissipation.^{3,6,14,38} We used TL to obtain information about stored energy and defect accumulation in the bulk of the oxide. TL is an electron–hole or hole–electron recombination luminescence of the preirradiated samples. It is generated during thermal annealing and thermal ionization of electron- and/or hole-type radiation defects.^{39–42}

We also used TL for experiments on water radiolysis on alkali halide crystal (AHC) surfaces.⁴³ The proposed mechanism involves thermalized electrons migrating to the surface, reacting with the water molecule, and producing hydrogen.^{3,13,14,43} Therefore, comparison with data on AHC can help understand the energy transfer mechanism in oxides.

Irradiated ZrO₂ microcrystals emit TL with a spectral maximum at 520 ± 20 nm and two thermo peaks at 410 ± 20 K and 510 ± 20 K (see the inset in Figure 6). These results very closely agree with published data for sintered ZrO₂.⁴⁴ The TL yield saturates at a quite low absorption dose (~ 1 kGy, see Figure 6). This usually happens when electrons and/or holes fill preexisting traps, and the efficiency of the additional radiation defects/traps production is low.

The anion vacancy is one of the most effective traps for the electrons in zirconia.⁴⁵ Electrons fill these anion vacancies, thus producing F and F⁺ centers.^{46,47} Thermal treatment of the sample at different oxygen pressures can change the oxygen vacancy concentration. In our experiment, quenching in the 10^{-2} Torr

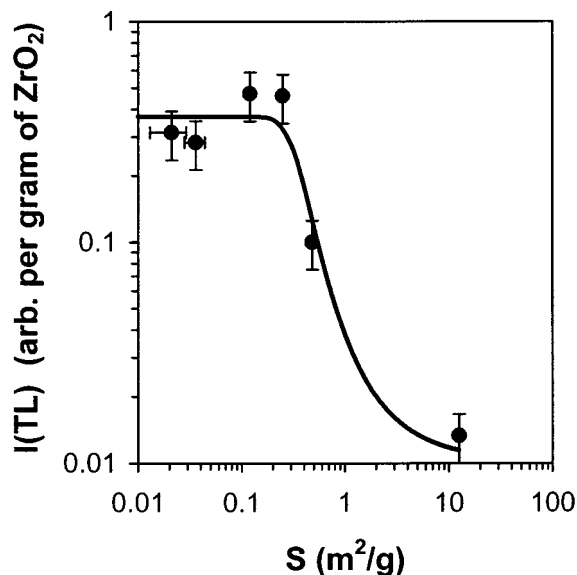


Figure 7. TL yield for peak (1) per gram of ZrO_2 vs the oxide specific area. $D_\gamma = 0.25$ MGy.

vacuum of the preannealed sample increased the yield of the main TL peak by a factor of 4 ± 1 vs the sample annealed in ambient air environment. The equilibrium concentration of anion vacancies V_{O}^{2+} in oxides depends on the partial pressure of oxygen p_{O_2} in gas phase as^{37,48}

$$V_{\text{O}}^{2+} \propto (p_{\text{O}_2})^{-1/6} \quad (1)$$

For the given experimental conditions, we expect a 5-fold increase in the oxygen vacancy concentration, which indicates that the TL yield is being limited by the number of electrons trapped in anion vacancies, as described in the following relationships

$$I_{\text{TL}} \propto k \times F \times V \quad (2)$$

$$F_\infty \propto V_{\text{O}}^{2+} \quad (3)$$

where I_{TL} is the TL yield, F and V are the concentrations of the electron and hole centers, k is a constant, and F_∞ is the concentration of the electron centers at the “saturating” dose.

Figure 7 shows the dependence of the TL yield on the ZrO_2 specific area. TL clearly is quenched in the given range of crystal dispersions as a result of the trapping of electrons and holes by the surface states. This surface quenching does not depend on the water molecules adsorbed on the surface. No degradation of TL was observed when preirradiated “dry” crystals were stored in a wet atmosphere, and no hydrogen was detected after dosing of water on the “dry” surface of preirradiated ZrO_2 . In other words, the $\text{ZrO}_2/\text{H}_2\text{O}$ system does not show the features of the electron-transfer mechanism that were observed for the $\text{KI}/\text{H}_2\text{O}$ system.⁴³

The effect of Nb^{5+} concentration in ZrO_2 on the TL yield is illustrated in Figure 8. TL quenches dramatically with niobium doping. In general, doping of the crystal can influence the TL yield by affecting the emission yield and by affecting the number of traps for electrons and holes. We measured the radioluminescence (RL) yield of the $\text{ZrO}_2 \cdot \text{Nb}$ crystals induced by beta irradiation from $^{90}\text{Sr}-\text{Y}$. RL is mainly a result of recombination of electrons and holes that exist during irradiation,^{14,40} whereas TL is associated with electrons and holes trapped after irradiation. In contrast to TL, the RL was quenched only by

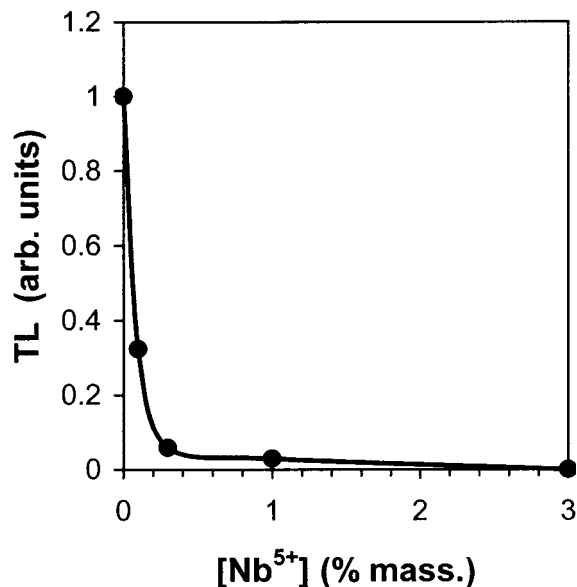
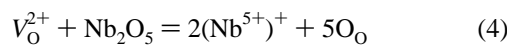


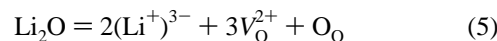
Figure 8. TL yield for peak (1) per gram of ZrO_2 vs concentration of Nb^{5+} in ZrO_2 . $D_\gamma = 0.5$ MGy.

40% for the highest Nb concentration (3% mass.). Two orders of magnitude quenching was observed for the TL of the same samples (see Figure 8). Hence, niobium affects mainly the trap concentration.

The equilibrium concentration of the oxygen vacancies in ZrO_2 (eq 1) should decrease with Nb(V) doping according to the charge and mass balance³⁷



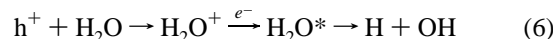
where $(\text{Nb}^{5+})^+$ is Nb^{5+} in the site of Zr^{4+} , and O_{O} is O^{2-} in an anion site. Therefore, the mechanism of TL quenching with niobium doping can be understood in terms of decreasing of oxygen vacancy concentration (i.e., electron trap concentration, see eq 2–4). Experiments with Li^+ doping are consistent with this model. Doping ZrO_2 with Li^+ should increase concentration of anion vacancies according to the following equation³⁷



where $(\text{Li}^+)^{3-}$ is Li^+ in the site of Zr^{4+} . In experiments, ZrO_2 crystals doped with 0.1% mass Li^+ have twice the TL yield than undoped samples. Thus, doping with Nb^{5+} and Li^+ yield an opposite effect on the trapping of electrons and holes in bulk ZrO_2 .

4. Discussion

A. Hydrogen Yield–Band-Gap Correlation. Band-gap energy is a fundamental parameter that affects various radiation-induced processes on the surface of insulators and semiconductors.^{49,50} Two main types of “band-gap” dependence are discussed in the literature: threshold-type (or steplike) and resonance-type. Threshold-type dependence is reported for mechanisms involving recombination of a band electron with a hole (or a hole with an electron) on the adsorbed molecule.^{6,9,10,19} For H_2O on Al_2O_3 , the following reactions were proposed⁵¹



Recombination energy, deposited on the molecule, is close to

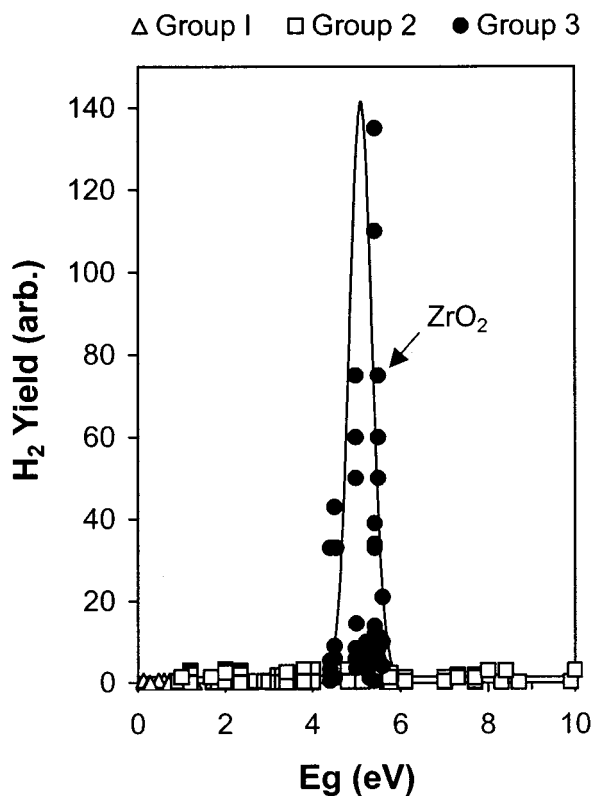


Figure 9. Hydrogen radiation chemical yield vs oxide band gap for radiolysis of H_2O molecules adsorbed on the surface of various oxides with coverage 1 ± 0.4 ML. $G(\text{H}_2)$ is calculated on an electron fraction basis relative to the energy of γ rays directly absorbed by the H_2O molecules. Three groups of oxides are marked differently (see above the section 3A for the oxide/group designation). Group 1 oxides are inhibitors, group 2 – indifferent, and group 3 – promoters for the adsorbed water radiolysis. Several data points represent each oxide (see section 3A for details).

the matrix band gap and should be higher than the molecule bond-breaking energy. Many details of this process including O_2 creation are not clear yet.

Resonant-type dependence is suggested for the exciton transfer process.^{15–17,52} Exciton transfer was proposed for N_2O radiolysis on the ZrO_2 and Al_2O_3 surfaces at 77 K.^{8,15–17} According to the Förster theory,^{53,52} an exciton transfer occurs due to a weak dipole–dipole coupling in the condensed state. The donor (oxide) exciton spectrum should overlap the dissociative excitation spectrum of the acceptor (the adsorbed molecule). The energy of the fundamental exciton is typically a little lower than the band gap energy. In semiconductors, the energy transfers by the coherent excitons (wave packets), for which mobility is very high due to relatively weak exciton–phonon coupling and low effective mass.⁵² Excitons can self-trap in BeO , SiO_2 , GeO_2 , MgO , Li_2O , and other oxides due to exciton–lattice coupling.^{54–57} Unfortunately, there is no information reported on the free or localized exciton coupling with adsorbed water molecules.

Figure 9 presents our data on the hydrogen yields from various oxides plotted vs the oxide band gap. For most of the oxides, we used spectroscopic data published by Strehlow and Cook⁵⁸ for the band gap. A more extended search for information on ZrO_2 yielded band-gap data that ranged from 5 to 5.5 eV.^{47,59–63} For La_2O_3 and rare-earth element oxides, we used published data.^{49,64,65} Unrealistically low data from conductivity measurements for Sm_2O_3 , Eu_2O_3 , and Er_2O_3 (1.17, 1.7, and 1.4 eV respectively) were not used.⁵⁸ The spectroscopic data from^{49,64,65} were utilized instead (5.0, 4.5, and 5.4 eV respec-

tively). Band-gap data reported in the literature, even for the same material, often varies significantly, which is reflected on the plot. As mentioned above, data on hydrogen yield also vary because of factors other than band gap that control the process. Each specific oxide shown in Figure 9 is represented by several data points: all the G values obtained in this work for different oxide stocks and under different conditions, duplicated for the maximum and minimum E_g value found from the literature (e.g., 5 and 5.5 eV for ZrO_2 , 3 and 3.75 eV for TiO_2 , etc.). The plot shows a resonant maximum near $E_g = 5$ eV. All “oxide-promoters” have band gaps within the range from 4.5 to 6 eV. Some degree of uncertainty in the real band gaps of the studied materials, changes in the band gap at the surface, and other factors may affect the peak position and width. The resonant character of the “ H_2 yield vs band gap” dependence is consistent with an exciton transfer mechanism.^{15,16,17}

B. Water Molecule Dissociation. The energy of the H–OH bond in the water molecule is 5.1 eV.⁶⁶ However, the dissociative excitation thresholds for homogeneous vapor, liquid, and solid water are significantly higher. The VUV absorption spectrum of H_2O vapor⁶⁷ shows a first band with a maximum at ~ 7.45 eV and an absorption threshold near 6.6 eV. In the spectrum of liquid water, the lowest transition appears to be shifted to higher energies, with a maximum at 8.2 eV and exponential tail extending to 5.9 eV.⁶⁷ The liquid water photoionization quantum yield for one-photon excitation near the absorption edge at 6.4 eV is 1.3%.⁶⁸ The threshold value for the $^1\text{B}_1$ excitation in ice is 7.2 eV.^{69,70} At values below the electronic excitation threshold, H_2 can be produced from water directly via a dissociative electron attachment (DEA) with threshold at ~ 6.3 eV.⁷¹ Hence, the primary electronic excitations in the ZrO_2 lattice (excitons or electron–hole pairs) are not energetic enough to dissociate a physisorbed water molecule, which is consistent with our observations.

Photocatalytic decomposition of water on the oxide surface typically involves excitation of the catalyst and H_2O molecules strongly bound to the surface, which yields a lower dissociation threshold.⁷² The lowest reported energy of the UV quanta active for the photocatalytic splitting of adsorbed water is 4 eV.⁷² H and OH radicals are typically primary products of water photolysis on the oxide surface.⁷² The most radiation-labile first chemisorbed state of water (~ 400 K TPD maximum for ZrO_2) may have a lower dissociation threshold, being altered as result of interaction with surface ions.³⁴ This state has been observed in the TPD spectrum of D_2O submonolayer on the surface of a thin ZrO_2 film^{73,74} and is associated with a nondissociated water molecule, adsorbed on a surface defect (tentatively on the anion vacancy). The reported desorption energy for such a molecule is 89 kJ/mol (~ 1 eV).⁷³ Our data show a high effective “landing” area for this chemisorbed water (~ 25 Å² per molecule), which indicates that the H_2O molecules are localized on particular sites of the ZrO_2 surface (probably at defect sites).³⁵ Because this state is not dissociated, a significant part of the adsorption energy should be attributed to deformation of the molecular structure. This energy may close the gap between the dissociation threshold for the free water molecule and the ZrO_2 fundamental exciton energy (5 to 5.5 eV). The exciton mechanism is consistent with reported observations of water photodecomposition with 254 nm (4.9 eV) UV photons in ZrO_2 /water suspensions.^{22,23} The reported 4.9 eV value is close to the exciton absorption maximum in ZrO_2 , but lower than the band gap (i.e., an onset for electron–hole pair production).

Our experimental technique did not allow us to detect the primary products of the water molecule dissociation. The

analyzed H₂ is likely the product of the H atom recombination (eq 7). We did not monitor the oxygen species, but we expect that production of O₂ is consistent with reported photolysis data for the ZrO₂/water system.^{22,23} There is no clear mechanism reported for O₂ creation during adsorbed water photolysis or radiolysis. In liquid water, O₂ is a product of the OH radical recombination to H₂O₂, generation of HO₂ radicals and their recombination.^{30,31} We also can expect an oxide catalyzed H₂O₂ decomposition that yields O₂.

The high-temperature peak of the water TPD should be associated with the surface hydroxyl groups.^{27,75} Hydroxyls, as well as physisorbed water, are much more stable under irradiation, probably because their dissociation thresholds are higher than the energy of the ZrO₂ exciton.

C. Bulk–Surface Energy Exchange. An electronic excitation (electron, hole, exciton), produced at some point of the crystal lattice, has an average lifetime depending on the reactions of recombination (or annihilation for excitons) and trapping

$$1/\tau = 1/\tau_{rec} + 1/\tau_{trap} \quad (8)$$

The average diffusion displacement during a lifetime will be

$$L = \sqrt{4D\tau} \quad (9)$$

where D is a diffusion coefficient. If some part of the surface is inside a sphere with radius L , the diffusing excitation could be trapped on the surface or could react with adsorbed species. To explain this process, we propose a simple model of a spherical crystal particle with radius R and outer layer with thickness L . We assume that certain excitation can be produced by radiation with equal probability anywhere within the crystal. There are two possibilities for the excitation:

(1) to recombine or to be trapped in the bulk of the crystal with yield I , if the excitation was created in the sphere with radius $(R - L)$

(2) to react with the adsorbed molecule or to be trapped on the surface with 100% probability and with yield G , if the excitation was created in the subsurface layer L .

Simple geometric considerations give the following expressions for the yields of the bulk and the surface reactions per unit of the crystal mass vs crystal radius for $R \geq L$

$$I = I_{\infty} \left(1 - \frac{L}{R}\right)^3 \quad (10)$$

$$G = G_0 \left(1 - \left(1 - \frac{L}{R}\right)^3\right) \quad (11)$$

where I_{∞} is a yield of the oxide electronic excitations per unit of the oxide mass for the large crystals with $R \gg L$; and G_0 is a hydrogen yield from the water adsorbed on the “small” crystals with $R = L$, i.e., for the system, where all the excitations created in the oxide, react with the water molecules at the surface.

For crystals with $R \gg L$ we will have

$$I = I_{\infty} = \text{const} \quad (12)$$

$$G \approx G_0 \times \frac{3L}{R} = G_0 \times L \times S_{SP} \times \rho \quad (13)$$

where S_{SP} is a specific area of the crystals (m²/g)

$$S_{SP} = \frac{3}{\rho R} \quad (14)$$

and ρ is density. For the crystals with $R = L$, we will have $I =$

0 and $G = G_0 = \text{const}$. Hence, changing the crystal size (or specific area) allows evaluation of parameters such as diffusion displacement and lifetime, which are fundamental parameters of electronic excitations.

Our data (Figures 4 and 7) do not show a correlation between radiation-induced processes on the surface (H₂) and in the bulk (TL). The migration distance $L(\text{TL})$ for the TL surface quenching is larger than $L(\text{H}_2)$ for the hydrogen production. The latter distance is less than the smallest crystal size used in our experiment (see eq 13). This result can be compared to data obtained by Sagert et al.⁸ for the ZrO₂/N₂O system, where maximal yields of the N₂O radiolysis were obtained for much more disperse ZrO₂ samples with $S_{SP} > 90 \text{ m}^2 \text{ g}^{-1}$, and the authors attributed the result to *exciton transfer*. Using eq 14, the exciton migration distance was evaluated to be $\sim 5 \text{ nm}$.⁸ Solid lines in Figures 4 and 7 are approximations from eq 10, 11, and 14 for $L(\text{H}_2) \cong 5 \text{ nm}$ and $L(\text{TL}) = 26 \pm 4 \text{ nm}$. Therefore, differences in the migration distances could be associated with different types of mobile electronic excitations involved in both processes: electrons and holes for the TL and excitons for the H₂ production.

The KI/H₂O system with an alternative electron–hole mechanism of the energy migration shows identical L values obtained from the TL, RL, and H₂ production experiments with similar experimental arrangement.^{3–5,13,14,43,76}

TL and H₂ production also do not correlate in the experiments with doping of the ZrO₂ crystals. Doping with Nb⁵⁺ and Li⁺ changes concentration of the anion vacancy–trap for the electrons, as seen in the TL experiments. Less efficient trapping in the bulk (niobium doping) should *increase* the lifetime of the electrons and their flux to the surface and vice versa (eqs 8, 9, 11, and 13). The observed *decrease* of the H₂ production with niobium doping (Figure 5) is another indication that electrons are not involved in this process. The minimal concentration of niobium $\sim 0.1\%$, used in our experiment, corresponds to the average distance of $\sim 3 \text{ nm}$ between the Nb⁵⁺ ions.⁷⁷ This number is close to the 5 nm value obtained from the dispersion experiments⁸ and also allows evaluation of the exciton migration distance. Hence, the doping experiments are consistent with the exciton mechanism of energy migration to the adsorbed water molecule.

D. Surface Enhancement of Water Radiolysis and Radiation-Induced Oxidation of Zirconium. The opposite effects of niobium and lithium on energy transfer in the ZrO₂/H₂O system may have a similar mechanistic basis as the known opposite effects of those elements on the radiation-induced oxidation of zirconium-based alloys in high temperature water. From many tested Zr-based alloys and pure zirconium, only niobium-doped materials typically show no radiation enhancement of oxidation in high-temperature water.^{78,79} TL experiments⁴¹ show that niobium incorporates into the ZrO₂ oxide film onto those alloys and remarkably effects lifetimes and migration distances of the electronic excitations created by irradiation. On the other hand, LiOH dosing into water is known as a promoter of Zircaloy cladding oxidation due to incorporation of Li⁺ cations into the protective ZrO₂ oxide film.⁸⁰ Such behavior may be another indication of the important role that water radiolysis plays in the corrosion enhancement of zirconium-based nuclear fuel cladding.^{78,80–86} According to the data presented in this work, radiolysis of water coolant should be enhanced near the fuel cladding surface due to energy transfer from the zirconium oxide. The energy transfer is very sensitive to the presence of Nb⁵⁺ or Li⁺ incorporated into the protective ZrO₂ film.

5. Conclusion

According to the radiation-chemical yield, oxides can be generally classified into three groups: I. Oxides that lower the H₂ yield (MnO₂, Co₃O₄, CuO, and Fe₂O₃); II. Oxides with H₂ yields that are close to *G* values obtained in control experiments (MgO, CaO, SrO, BaO, ZnO, CdO, Cu₂O, NiO, Cr₂O₃, Al₂O₃, CeO₂, SiO₂, TiO₂, Nb₂O₅, and WO₃); and III. Oxides that can increase the H₂ yield as compared with the radiolysis of water without oxides (Ga₂O₃, Y₂O₃, La₂O₃, Nd₂O₃, Sm₂O₃, Eu₂O₃, Gd₂O₃, Yb₂O₃, Er₂O₃, HfO₂, and ZrO₂). For the third group, the H₂ yield can be much greater than for the homogeneous process due to effective energy transfer at the oxide/water interface. There are several parameters, such as the oxide band-gap, water adsorption form, and energy migration distance, that can contribute collectively to “enhanced” radiolysis yields at interfaces. We present data of “effective” *G*(H₂) vs band-gap (*E_g*) energy that shows a resonant maximum at *E_g* = 5 eV. This corresponds to the energy of the H–OH bond in the water molecule (5.1 eV). We also demonstrate that variation of the ZrO₂ specific area in a range from 0.02 to 12 m² g⁻¹ shows that the H₂ yield per unit area of the crystal surface is constant. Doping the ZrO₂ bulk with Nb⁵⁺ and Li⁺ ions remarkably affects the H₂ yield. We estimated the energy migration distance to be ~5 nm. Finally, thermostimulated luminescence was used to probe the nature of migrating electronic excitations in ZrO₂. We propose a mechanism for the adsorbed water radiolysis based on the migration of excitons to the surface and their resonant coupling with the H₂O adsorption complex. We do not exclude other possible mechanisms of energy transfer at the oxide/water interface, but we consider them less effective for H₂ production.

Acknowledgment. The authors are glad to thank A.Yu. Bychkov, for help with TL measurements; Profs. A.F. Nechaev, V.M. Sedov, A.A. Persinen, I.A. Vassiliev, T.M. Orlando, and Dr. S. A. Joyce -for help and useful discussions. Experimental work was performed at the Institute of Technology, Saint Petersburg, Russia and was supported by the Russian Ministry of Atomic Energy. Data analysis and preparation of the manuscript were performed at the W. R. Wiley, Environmental Molecular Sciences Laboratory, located at Pacific Northwest National Laboratory (PNNL). PNNL is operated by Battelle for the U.S. Department of Energy (DOE). This part of the work was supported by DOE’s Environmental Management Science Program.

References and Notes

- Schatz, T.; Cook, A. R.; Meisel, D. *J. Phys. Chem. B* **1999**, *103*, 10 209–10 213.
- Schatz, T.; Cook, A. R.; Meisel, D. *J. Phys. Chem. B* **1998**, *102*, 7225–7230.
- Alexandrov, A. B.; Gusev, A. L.; Petrik, N. G. *Russian, J. Phys. Chem.* **1987**, *61*, 198.
- Alexandrov, A. B.; Bychkov, A. Y.; Vall, A. I.; Petrik, N. G.; Sedov, V. M. *Russian J. Phys. Chem.* **1991**, *65*, 1604–1608.
- Nechaev, A. F. *Radiat. Phys. Chem.* **1986**, *28*, 433–436.
- Rabe, J. G.; Rabe, B.; Allen, A. O. *J. Phys. Chem.* **1966**, *70*, 1098–1107.
- Sagert, N. H.; Dyne, P. J. *Canad. Journ. of Chem.* **1967**, *45*, 615–627.
- Sagert, N. H.; Robinson, R. W. *Canad. Journ. of Chem.* **1968**, *46*, 2075–2080.
- Zhabrova, G. M.; Vladimirova, V. I. *Russian Chemical Review* **1969**, *38*, 330–344.
- Khare, M.; Johnson, E. R. *J. Phys. Chem.* **1970**, *74*, 4085–4091.
- Auger Electron Spectroscopy*; Briant, C. L., Messmer, R. P., Eds.; Academic Press: Boston, 1988; Vol. 30.
- Elango, M.; Prουλmann, J.; Zhurakovskii, A. P. *Phys. Stat. Sol. (b)* **1983**, *115*, 399–407.

- Alexandrov, A. B.; Nechaev, A. F. *Russian J. Phys. Chem.* **1984**, *58*, 1108.
- Aluker, E. D.; Nesterova, S. N.; Nechaev, A. F. *Soviet Physics—Solid State* **1988**, *30*, 596–599.
- Volkov, A. I.; Volkova, G. G.; Yermolaev, V. K.; Sazonov, L. A. *React. Kinet. Catal. Lett.* **1982**, *20*, 277–282.
- Volkov, A. I.; Volkova, G. G.; Yermolaev, V. K.; Sazonov, L. A. *React. Kinet. Catal. Lett.* **1982**, *20*, 283–288.
- Volkov, A. I.; Sazonov, L. A. *React. Kinet. Catal. Lett.* **1982**, *20*, 289–292.
- Aristov, Y. I.; Volkov, A. I.; Parmon, V. N.; Zamaraev, K. I. *React. Kinet. Catal. Lett.* **1984**, *25*, 329–334.
- Garibov, A. A. “Water Radiolysis in the Presence of Oxides”; 5-th Tihany Symposium on Radiation Chemistry, 1983, Tihany, Hungary.
- Abe, T.; Suzuki, E.; Nagoshi, K.; Miyashita, K.; Kaneko, M. *J. Phys. Chem. B* **1999**, *103*, 1119–1123.
- Gratzel, M. *Acc. Chem. Res.* **1981**, *14*, 376–384.
- Sayama, K.; Arakawa, H. *J. Phys. Chem.* **1993**, *97*, 531–533.
- Sayama, K.; Arakawa, H. *J. Photochem. Photobiol., A* **1994**, *77*, 243–7.
- Serpone, N.; Pelizzetti, E.; Gratzel, M. *Coord. Chem. Rev.* **1985**, *64*, 225–245.
- Zhang, Z.; Wang, C.-C.; Zakaria, R.; Ying, J. Y. *J. Phys. Chem. B* **1998**, *102*, 10 871–10 878.
- Petrik, N. G.; Alexandrov, A. B.; Orlando, T. M.; Vall, A. I. *Trans. ANS* **1999**, *81*, 101–102.
- Gregg, S. J.; Sing, K. S. W. *Adsorption, Surface Area and Porosity*; Academic Press: London; New York, 1982.
- Hillebrand, W. F.; Lundell, G. E. F. *Applied Inorganic Analysis; with Special Reference to the Analysis of Metals, Minerals, and Rocks*; Wiley: New York, 1953.
- Kase, K. R. *The Dosimetry of Ionizing Radiation*; Academic Press: Orlando, 1985; Vol. 1.
- Henley, E. J.; Johnson, E. R. *The Chemistry and Physics of High Energy Reactions*; University Press: Washington, DC, 1969.
- Pikaev, A. K. *Modern Radiation Chemistry. Radiolysis of Gases and Liquids*; Nauka: Moscow, 1986.
- Willis, C.; Boyd, A. W. *Radiat. Phys. Chem.* **1976**, *8*, 71–111.
- Anderson, A. R.; Knight, B.; Winter, J. A. *Trans. Faraday Soc.* **1966**, *62*, 359–370.
- Thiel, P. A.; Madey, T. E. *Surface Science Reports* **1987**, *7*, 211–385.
- Hall, P. G.; Langran-Goldsmith, H. *J. Phys. Chem.* **1992**, *96*, 867–870.
- Holmes, H. F.; Fuller, E. L.; Beh, R. A. *J. Colloid Interface Sci.* **1974**, *47*, 365–371.
- Kofstad, P. *Nonstoichiometry, Diffusion and Electrical Conductivity in Binary Metal Oxides*; Wiley-Interscience: New York, 1972.
- Wong, P. K.; Willard, J. E. *J. Phys. Chem.* **1968**, *72*, 2623–2627.
- Chang, S.-C.; Su, C.-S. *Radiat. Prot. Dosim.* **1993**, *47*, 169–172.
- Curie, D. *Luminescence in crystals*; Methuen & Co Ltd; John Wiley & Sons Inc.: London, New York, 1963.
- Bychkov, A. Y.; Petrik, N. G.; Alexandrov, A. B.; Nechaev, A. F. “Thermoluminescence of Oxidized Zr and Zr Alloys”; Fundamental Aspects of Corrosion of Zirconium Based Alloys in Water Reactor Environments, IAEA Tech. Com. Meet., 1989, Portland, OR.
- Antonov-Romanovskii, V. V. *Phys. Stat. Sol.* **1968**, *30*, 341–347.
- Sedov, V. M.; Alexandrov, A. B.; Rulev, Y. P.; Nechaev, A. F. *Soviet Technical Physics Lett.* **1984**, *10*, 530–531.
- Chang, S.-C.; Su, C.-S. *Radiat. Prot. Dosim.* **1993**, *47*, 187–189.
- Petrik, N. G.; Taylor, D. P.; Orlando, T. M. *Journ. Appl. Phys.* **1999**, *85*, 6770–6776.
- Choi, S.; Takeuchi, T. *Phys. Rev. Lett.* **1983**, *50*, 1474–1477.
- PaiVerneker, V. R.; Petelin, A. N.; Crowne, F. J.; Nagle, D. C. *Phys. Rev. B* **1989**, *40*, 8555–8557.
- Yamawaki, M.; Suzuki, A.; Ono, F.; Yamaguchi, K. *J. Nucl. Mater.* **1997**, *248*, 3190–0322.
- Emeline, A. V.; Kataeva, G. V.; Ryabchuk, V. K.; Serpone, N. J. *Phys. Chem. B* **1999**, *103*, 9190–9199.
- Emeline, A. V.; Kuzmin, G. N.; Purevdorj, D.; Ryabchuk, V. K.; Serpone, N. J. *Phys. Chem. B* **2000**, *104*, 2989–2999.
- Garibov, A. A.; Parmon, V. N.; Agaev, T. N.; Kasumov, R. D. *High En. Chem.* **1991**, *25*, 86–90.
- Agranovich, V. M.; Galanin, M. D. *Electronic Excitation Energy Transfer in Condensed States*; Nauka: Moscow, 1978.
- Förster, T. *Discuss. Faraday Soc.* **1959**, *27*, 7.
- Shluger, A. L.; Harker, A. H.; Grimes, R. W.; Catlow, C. R. A. *Philos. Trans. R. Soc. London A* **1992**, *341*, 221–231.
- Bautin, K. V.; Kudiyakov, S. V.; Ogorodnikov, I. N.; Kruzhalov, A. V.; Yakovlev, V. Y. *J. of Luminescence* **1998**, *76&77*, 467–469.
- Itoh, N. *Nucl. Instrum. and Methods Phys. Res. B* **1996**, *116*, 33 36.

- (57) Itoh, N.; Tanimura, K.; Trukhin, A. N. *Nucl. Instrum. and Methods Phys. Res. B* **1996**, *116*, 72–76.
- (58) Strehlow, W. H.; Cook, E. L. *J. Phys. Chem. Ref. Data* **1973**, *2*, 163–199.
- (59) Králik, B.; Chang, E. K.; Louie, S. G. *Phys. Rev. B* **1998**, *57*, 7027–7035.
- (60) Kwok, C.-K.; Aita, C. R. *J. Appl. Phys.* **1989**, *66*, 2756–2758.
- (61) Petrik, N. G.; Taylor, D. P.; Simpson, W. C.; Orlando, T. M. "Laser-Stimulated Luminescence of Yttria-Stabilized Cubic Zirconia Crystals"; 9-th Ann. Pacific Northwest Symposium of the American Vacuum Society, 1997, Troutdale, OR.
- (62) Stefanovich, E. V.; Shluger, A. L.; Catlow, C. R. A. *Phys. Rev. B* **1994**, *49*, 11 560–11 571.
- (63) Camagni, P.; Samoggia, G.; Sangaletti, L.; Parmigiani, F.; Zema, N. *Phys. Rev. B* **1994**, *50*, 4292–4296.
- (64) Prokof'ev, A. V.; Shelykh, A. I.; Smirnov, I. A.; Melekh, B. T. *Phys. Solid State* **1996**, *38*, 1502–1504.
- (65) *Physical and Chemical Properties of the Oxides. Handbook*; 2nd ed.; Samsonov, G. V., Ed.; Metallurgy: Moscow, 1978; p 472.
- (66) *CRC Handbook of Chemistry and Physics*; Lide, D. R., Frederikse, H. P. R., Eds.; CRC: Boca Raton–New York–London–Tokyo, 1995.
- (67) Sander, M. U.; Luter, K.; Troe, J. *Ber. Bunsen-Ges. Phys. Chem.* **1993**, *97*, 953–961.
- (68) Bartels, D. M.; Crowell, R. A. *J. Phys. Chem. A* **2000**, *104*, 3349–3355.
- (69) Robin, M. B. *Higher Excited States of Polyatomic Molecules*; Academic Press: New York, 1974; Vol. 1.
- (70) Klyachko, D. V.; Rowntree, P.; Sanche, L. *Surface Science* **1997**, *389*, 29–47.
- (71) Kimmel, G. A.; Orlando, T. M.; Vézina, C.; Sanche, L. *J. Chem. Phys.* **1994**, *101*, 3282–3286.
- (72) Solonitsyn, Y. P.; Basov, L. L.; Ryabchuk, V. K. *Russian, J. Phys. Chem.* **1980**, *54*, 1494–1496.
- (73) Maurice, V.; Takeuchi, K.; Salmeron, M.; Somorjai, G. A. *Surf. Sci.* **1991**, *250*, 99–111.
- (74) Takeuchi, K.; Perry, S. S.; Salmeron, M.; Somorjai, G. A. *Surf. Sci.* **1995**, *323*, 30–38.
- (75) Orlando, R.; Pisani, C.; Ruiz, E.; Sautet, P. *Surf. Sci.* **1992**, *275*, 482–492.
- (76) Alexandrov, A. B.; Aluker, E. D.; Vassiliev, I. A.; Nechaev, A. F.; Chernov, S. A. *Introduction into Radiation Physics and Chemistry of Surface of Alkali Halide Crystals*; Zinatne: Riga, Latvia, 1989.
- (77) Ozawa, L.; Hersh, H. N. *Phys. Rev. Lett.* **1976**, *36*, 683–686.
- (78) Bradhurst, D. H.; Shirvington, P. J.; Heuer, P. M. *J. Nucl. Mater.* **1973**, *46*, 53–76.
- (79) Urbanic, V. F.; LeSurf, J. E.; Johnson, A. B. *J. Corrosion* **1973**, *31*, 15–20.
- (80) Billot, P.; Cox, B.; Ishigure, K.; Johnson, A. B.; Lemaignan, C.; Nechaev, A. F.; Petrik, N. G.; Reznichenko, E. A.; Ritchie, I. G.; Sukhanov, G. I. "Corrosion of Zirconium Alloys in Nuclear Power Plants," IAEA-TECDOC-684, 1993.
- (81) Burns, W. G.; Moore, P. B. *Radiat. Eff.* **1976**, *30*, 233–242.
- (82) Cox, B.; Ishigure, K.; Lemaignan, C.; Johnson, A. B.; Nechaev, A. F.; Petrik, N. G.; Reznichenko, E. A. "Mechanistic Understanding of Irradiation Corrosion of Zirconium Alloys in Nuclear Power Plants: Stimuli, Status and Outlook"; International Conference on Radiation Material Science, 1990, Alushta, SU.
- (83) Petrik, N. G. *High En. Chem.* **1997**, *31*, 368–372.
- (84) Petrik, N. G. *High En. Chem.* **1998**, *32*, 1–4.
- (85) Lemaignan, C. *J. Nucl. Mater.* **1992**, *187*, 122–130.
- (86) Cox, B. *J. Nucl. Mater.* **1968**, *1968*, 1–47.